https://doi.org/10.62836/iaet.v5i1.0007

Global Science Publishing

IAET

Innovations in Applied Engineering and Technology

https://ojs.sgsci.org/journals/iaet

Article

Modeling and Geometric Characteristics of a Circular-Arc-Profile and Circular-Arc-Tooth-Trace Cylindrical Gear Generated by Complementary Circular-Arc Cutters

Qi Zhang * and Li Hou

School of Mechanical Engineering, Sichuan University, Chengdu 610065, China

Abstract: To improve the limited flexibility in tooth-surface geometry control of circular-arc-tooth-trace cylindrical gears, a circular-arc-profile and circular-arc-tooth-trace cylindrical gear (C2CATT) generated by a pair of complementary, locally conjugate circular-arc cutters is proposed. Based on the machining principle of a dual-edge rotary cutter head, the cutter swept-surface equations, cutter-workpiece meshing equation, and parametric tooth-surface models are established. The effects of the main parameters on the middle-section tooth profile and tooth-trace geometric offset are then investigated. The results show that the tooth-trace geometric offset is symmetric about the mid-facewidth section, and its amplitude gradually decreases from the middle toward both ends. When the number of teeth increases from 31 to 67, the maximum offset amplitude decreases by 52.7%; when the module increases from 2 mm to 5 mm, it increases by 20.0%. Increasing the cutter-head radius effectively reduces the maximum offset amplitude. The pressure angle mainly affects the addendum, dedendum, and working tooth profile, whereas the cutter profile arc radius and root fillet coefficient primarily affect the local transition regions. The proposed model and the obtained parameter relationships provide a theoretical basis for tooth-surface design and cutter parameter selection of C2CATT gears.

Keywords: circular-arc profile; circular-arc-tooth-trace cylindrical gear; complementary circular-arc cutter; rotary cutter head; tooth-surface modeling; geometric characteristics

1. Introduction

Gear transmissions are developing toward higher power density, higher precision, lower vibration and noise, and greater reliability. Complex operating conditions demand not only favorable load-carrying and meshing performance, but also tooth-surface geometries that are designable, manufacturable, and tolerant of errors. By introducing tooth-trace curvature along the facewidth, circular-arc-tooth-trace cylindrical gears provide an additional geometric degree of freedom for controlling the contact region, load distribution, and meshing behavior. Wu et al. investigated the contact characteristics of circular-arc curvilinear-tooth gear drives and clarified the relationship between tooth-surface geometry and the contact pattern [1]. Peng et al. proposed an arc-tooth-trace cycloid cylindrical gear, thereby extending the range of available tooth-surface configurations [2]. Zhang et al. demonstrated the design and manufacturing feasibility of circular-arc-tooth-trace cylindrical gears through analyses of machining, meshing, and contact [3]. For engineering implementation, Liang et al. developed a dedicated machine tool for VH-CATT cylindrical gears and experimentally examined the effects of

Received: 26 August 2026; Accepted: 9 September 2026.

* Corresponding: Qi Zhang (pzhuzq@126.com)

cutter-head speed, feed rate, and other process parameters on tooth-surface machining errors. They subsequently established mappings from geometric error sources in the machine tool to tooth-surface deviations, demonstrating that machine-tool motion accuracy and cutter pose errors directly affect the final tooth-surface geometry [4 – 6]. These studies indicate that circular-arc-tooth-trace gears offer substantial potential for geometric development and engineering application. An accurate description of the relationships among cutter geometry, generating motion, and tooth-surface shape is therefore fundamental to their precision design and manufacture.

Systematic studies have been conducted on the tooth-surface modeling and geometric configurations of circular-arc-tooth-trace cylindrical gears. From a manufacturing perspective, Wang et al. developed a mathematical model of an arc-tooth cylindrical gear and analyzed its strength [7]. Based on the forming principle of a rotary cutter head, Zhao et al. derived the tooth-surface equations and constructed a digital model; they subsequently developed a complete tooth-surface model comprising the working surface, root transition surface, and root cylinder, and analyzed the corresponding cutting conditions [8,9]. These studies represent three successive stages: manufacturing-oriented modeling, rotary-cutter forming models, and complete tooth-surface models. Chen et al. constructed tooth surfaces using conjugate-curve theory, providing a theoretical basis for the geometric design of complex conjugate surfaces [10]. Regarding specific tooth-surface configurations, Luo et al. analyzed the geometric characteristics of variable-hyperbolic circular-arc-tooth-trace cylindrical gears [11], Ma et al. reconstructed circular-arc-tooth-trace gear surfaces and analyzed their profile geometry [12], and Jiang et al. modeled a circular-arc-profile and circular-arc-tooth-trace cylindrical gear and conducted a preliminary load-carrying capacity analysis [13]. Collectively, these studies established a foundation extending from tooth-surface generation theory and digital modeling to geometric characterization.

As tooth-surface models matured, research shifted toward machining errors, tooth contact, and load-carrying performance. Wu et al. established a theoretical relationship between machine-tool errors and tooth-surface deviations in circular-arc-tooth-trace cylindrical gears, and evaluated the effects of individual error components [14]. Wei et al. investigated the geometric contact characteristics and parameter sensitivities of VH-CATT gears while accounting for machining errors, and subsequently examined the effects of different machine-tool errors on tooth contact [15,16]. Ma et al. studied the contact performance of VH-CATT gears under installation errors [17]. Regarding contact and load-carrying behavior, Guo et al. obtained an analytical solution for the contact characteristics of VH-CATT gears [18]. Ma et al. studied the loaded tooth-surface contact area of circular-arc-tooth-trace cylindrical gears [19] and further performed modification design and loaded tooth contact analysis [20]. Recent work has extended to contact-stress reliability [21], nonlinear dynamics of modified gears [22], and meshing characteristics under cutter errors [23]. Thus, research on circular-arc-tooth-trace gears is progressing from ideal geometric modeling toward coupled analyses of errors, loads, and dynamic behavior.

Despite these advances in tooth-surface modeling, machining-error analysis, and contact performance, several limitations remain. First, most existing models address involute, cycloidal, or other circular-arc-tooth-trace gears generated by specific cutters; a unified mathematical description from the generating cutter to the complete spatial surface of a gear combining a circular-arc profile with a circular-arc tooth trace remains insufficient. Second, existing studies generally focus on a single aspect, such as tooth contact, machining error, or load-carrying capacity. Systematic quantitative analyses of how the profile arc radius, tooth-trace curvature, and related structural parameters jointly affect tooth thickness, tooth height, tip width, and overall tooth-surface geometry are scarce. Finally, although preliminary modeling and load-carrying analyses have been reported for circular-arc-profile and circular-arc-tooth-trace gears, the generating-cutter geometry, spatial generation mechanism, and effects of key parameters on tooth shape require further investigation. A complete mathematical model is therefore needed to reveal the relationships between the principal design parameters and geometric characteristics of this gear type.

To address these issues, this study develops a mathematical modeling method for a circular-arc-profile and circular-arc-tooth-trace cylindrical gear. A generating cutter is first designed according to the target gear geometry, and its cutting-edge equations are established. The mathematical models of the working tooth surfaces and associated boundary curves are then derived from the relative motion and meshing constraints between the cutter and workpiece, enabling the three-dimensional tooth surfaces to be constructed. Finally, the effects of the principal cutter and gear parameters on the tooth-profile shape and key geometric dimensions are analyzed. The results provide a theoretical basis for parameter design, manufacturing implementation, and subsequent meshing-performance analysis.

2. Machining Principle of the C2CATT Gear

2.1. Dual-Edge Rotary Cutter-Head Machining Principle

The C2CATT gear is generated using a dual-edge rotary cutter head. The machining principle and coordinate systems are shown in Figure 1. During machining, the inner and outer cutting edges rotate with the cutter head about its axis and form the corresponding swept cutting surfaces. The gear blank rotates about its own axis while feeding in the prescribed direction. The coordinated rotation of the cutter head, rotation of the blank, and feed motion establishes a deterministic spatial generating relationship between the cutter swept surface and the blank, thereby generating the concave and convex flanks of the C2CATT gear.

To describe the spatial generating relationship, three coordinate systems are established: the fixed cutter coordinate system $S_t(O_{t\text{-}xtytzt})$, with basis vectors i_t, j_t, and k_t; the fixed workpiece coordinate system S_w ($O_{w\text{-}xwywzw}$), with basis vectors iw, jw, and kw; and the moving workpiece coordinate system S_g ($O_{g\text{-}xgygzg}$), with basis vectors i_g, j_g, and k_g. The pitch radius of the gear blank is R_g, the blank rotation angle is φ, the nominal cutter-head radius is R_t, the cutter-head rotation angle is θ, and the facewidth is B. The positive coordinate-axis and rotation directions and the initial cutter-workpiece positions are defined as shown in Figure 1.

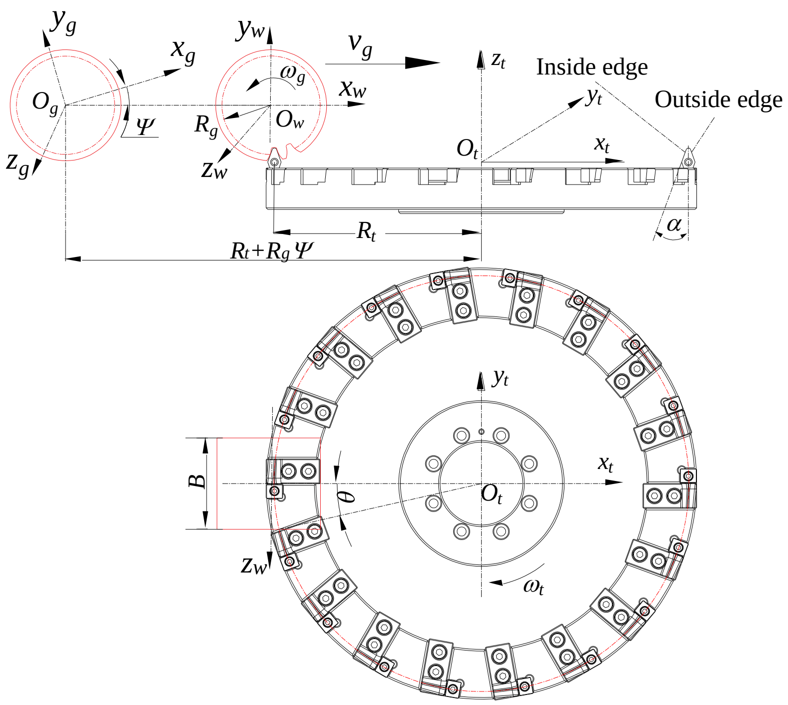

Figure 1. Machining Principle and Coordinate Systems of the C2CATT Gear.

During machining, the rotary cutter head is mounted on the machine-tool spindle and rotates about its axis at the angular velocity ω_t as the primary cutting motion. The inner and outer edges mounted on the cutter head rotate synchronously and form the inner and outer swept cutting surfaces, respectively, which generate the two flanks of a tooth space. Simultaneously, the gear blank rotates about its axis at the angular velocity ω_g and translates in the direction shown in Figure 1 at the feed velocity v_g. These motions define the cutter-workpiece relative motion, through which the cutting edges form the circular-arc tooth trace and envelope the corresponding tooth surfaces.

After one tooth space has been machined, the cutter is withdrawn and the blank is indexed about its axis through one angular pitch. The machining cycle is then repeated until all tooth spaces have been completed. Geometrically matched convex and concave circular-arc cutters are used to machine the driving and driven gears, respectively.

2.2. Complementary Locally Conjugate Circular-Arc Cutters

To generate the tooth surfaces of the driving and driven C2CATT gears, a geometrically matched pair of convex and concave circular-arc cutters is designed, as shown in Figure 2. The working edge of the convex cutter has an outwardly convex circular-arc profile, whereas that of the concave cutter has an inwardly concave profile. The two cutters satisfy a local conjugacy condition at the prescribed design contact position while retaining a curvature difference in the adjacent region. Consequently, the generated mating tooth surfaces satisfy the conjugacy condition only near the design position, providing a geometric basis for a localized-contact gear pair.

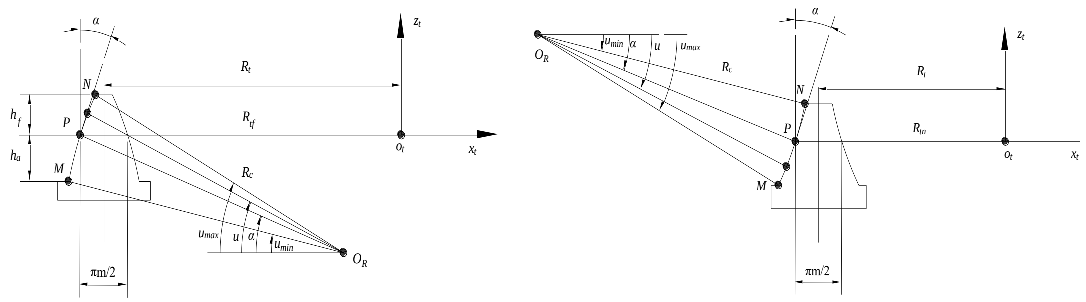

(a) Convex circular-arc cutter **(b)** Concave circular-arc cutter

Figure 2. Axial-Section Geometries and Parameters of the Complementary Convex and Concave Circular-Arc Cutters.

In Figure 2, α is the cutter pressure angle, m is the module of the gear to be machined, u is the angular parameter of a point on the cutting edge, and $u_{\min}$ and $u_{\max}$ are its lower and upper bounds, respectively. The parametric equations of the convex and concave circular-arc cutting edges are obtained from the geometry shown in Figure 2.

For the convex cutter,

$$u_{min} = \sin^{-1}\left(\frac{R_c \sin\alpha - h_a}{R_c}\right) u_{max} = \sin^{-1}\left(\frac{R_c \sin\alpha + h_f}{R_c}\right) \tag{1}$$

For the concave cutter,

$$u_{min} = \sin^{-1}\left(\frac{R_c \sin\alpha - h_f}{R_c}\right) u_{max} = \sin^{-1}\left(\frac{R_c \sin\alpha + h_a}{R_c}\right) \tag{2}$$

Equations (1) and (2) describe the circular-arc cutting edges of the convex and concave cutters in the axial section. The two cutters have the same module and nominal pressure angle. Their arc-center positions and radii are matched to provide a common normal direction at the design position. The convex and concave cutters have opposite curvature directions and a prescribed difference between their radii; this difference is transferred to the generated mating tooth surfaces and influences their local contact geometry.

3. Mathematical Model of the C2CATT Tooth Surfaces

3.1. Cutter Swept Surfaces

The C2CATT tooth-surface model is developed in three steps: construction of the cutter swept surfaces, solution of the cutter-workpiece meshing condition, and coordinate transformation. First, the swept surfaces are obtained by combining the convex and concave circular-arc cutting-edge equations with cutter-head rotation. Second, the meshing equation between each cutter swept surface and the gear blank is established from spatial meshing theory to determine the instantaneous contact line. Finally, the contact line is transformed from the cutter coordinate system to the coordinate system attached to the rotating blank, yielding the tooth-surface equations of the driving and driven gears. For an arbitrary point on the convex cutter, the swept surface expressed in St is

$$\boldsymbol{r}_{vex}^{(t)}=\begin{bmatrix}(-R_t\mp\frac{\pi}{4}m\pm R_c\cos\alpha\mp R_c\cos u)\cos\theta\\(-R_t\mp\frac{\pi}{4}m\pm R_c\cos\alpha\mp R_c\cos u)\sin\theta\\-R_c\sin\alpha+R_c\sin u\\1\end{bmatrix}\tag{3}$$

where the upper and lower signs represent the outer and inner cutting edges, respectively. R_c is the cutter profile arc radius. A positive coordinate is measured along the positive axis direction and a negative coordinate in the opposite direction. Correspondingly, an arbitrary point on the concave cutter swept surface is

$$\boldsymbol{r}_{cave}^{(t)}=\begin{bmatrix}(-R_t\mp\frac{\pi}{4}m\mp R_c\cos\alpha\pm R_c\cos u)\cos\theta\\(-R_t\mp\frac{\pi}{4}m\mp R_c\cos\alpha\pm R_c\cos u)\sin\theta\\R_c\sin\alpha-R_c\sin u\\1\end{bmatrix}\tag{4}$$

The vector forms of the convex and concave cutter swept surfaces in S_t are, respectively,

$$\begin{aligned}\boldsymbol{r}_{vex}^{(t)}=&(-R_t\mp\frac{\pi}{4}m\pm R_c\cos\alpha\mp R_c\cos u)\cos\theta\boldsymbol{i}_t-(R_c\sin\alpha-R_c\sin u)\boldsymbol{k}_t+\\&(-R_t\mp\frac{\pi}{4}m\pm R_c\cos\alpha\mp R_c\cos u)\sin\theta\boldsymbol{j}_t\end{aligned}\tag{5}$$

$$\begin{aligned}\boldsymbol{r}_{cave}^{(t)}=&(R_t\pm\frac{\pi}{4}m\pm R_c\cos\alpha\mp R_c\cos u)\cos\theta\boldsymbol{i}_t+(R_c\sin\alpha-R_c\sin u)\boldsymbol{k}_t+\\&(R_t\pm\frac{\pi}{4}m\pm R_c\cos\alpha\mp R_c\cos u)\sin\theta\boldsymbol{j}_t\end{aligned}\tag{6}$$

Taking the concave cutter as an example,

$$\begin{cases}\boldsymbol{r}_{du}=\dfrac{\partial\boldsymbol{r}_{cove}}{\partial u}=\pm R_c\sin u\cos\theta i_t\pm R_c\sin u\sin\theta\boldsymbol{j}_t-R_c\cos u\boldsymbol{k}_t\\\boldsymbol{r}_{d\theta}=\dfrac{\partial\boldsymbol{r}_{cove}}{\partial\theta}=(R_t\pm\frac{\pi}{4}m\pm R_c\cos\alpha\mp R_c\cos u)\left(-\sin\theta\boldsymbol{i}_t+\cos\theta\boldsymbol{j}_t\right)\end{cases}\tag{7}$$

The unit normal vector of the concave cutter swept surface, expressed in S_t, is obtained from

$$\begin{aligned}\boldsymbol{n}_t^{(t)}=&\frac{\partial\boldsymbol{r}_{cove}}{\partial u}\times\frac{\partial\boldsymbol{r}_{cove}}{\partial\theta}\\=&\begin{vmatrix}\boldsymbol{i}_t&\boldsymbol{j}_t&\boldsymbol{k}_t\\\pm R_c\sin u\cos\theta&\pm R_c\sin u\sin\theta&-R_c\cos u\\-\delta\sin\theta&\delta\cos\theta&0\end{vmatrix}\\=&\delta R_c(\cos u\cos\theta\boldsymbol{i}_t+\sin\theta\cos\theta\boldsymbol{j}_t\pm\sin u\boldsymbol{k}_t)\end{aligned}\tag{8}$$

Therefore, the unit normal vector is

$$\boldsymbol{e_t}=\cos u\cos\theta\boldsymbol{i}_t+\sin\theta\cos\theta\boldsymbol{j}_t\pm\sin u\boldsymbol{k}_t\tag{9}$$

3.2. Cutter-Workpiece Meshing Equation and Tooth-Surface Generation

Let $\boldsymbol{M}$ be an instantaneous contact point between the cutter swept surface and the gear blank. The velocities of the cutter and blank at $\boldsymbol{M}$, expressed in the fixed coordinate system St, are v_t and v_g, respectively. The cutter velocity relative to the blank is v_{tg}. According to spatial envelope theory, its component along the cutter-surface normal must vanish at an instantaneous contact point; hence,

$$\phi=\boldsymbol{n}_t\cdot\boldsymbol{v}_{tg}=\boldsymbol{n}_t\cdot\boldsymbol{v}_t-\boldsymbol{n}_t\cdot\boldsymbol{v}_g=0\tag{10}$$

In St, the position vectors from O_t and O_g to M and that from O_t to O_g are, respectively,

$$\boldsymbol{O}_t\boldsymbol{M}=\boldsymbol{r}_t,\boldsymbol{O}_g\boldsymbol{M}=\boldsymbol{r}_g,\boldsymbol{O}_g\boldsymbol{O}_t=\boldsymbol{\varepsilon}\tag{11}$$

$$\boldsymbol{r}_g=\boldsymbol{\varepsilon}+\boldsymbol{r}_t\tag{12}$$

$$\boldsymbol{\varepsilon}=(R_g\psi+R_t)\boldsymbol{i}_t-R_g\boldsymbol{k}_t\tag{13}$$

The cutter velocity at M is induced by the rotation of the cutter head about its axis and is expressed as

$$\begin{aligned}\boldsymbol{r}_g=&[-(R_t\pm\frac{\pi}{4}m\pm R_c\cos\alpha\mp R_c\cos u)\cos\theta+R_g\psi+R_t]\boldsymbol{i}_t-\\&(R_t\pm\frac{\pi}{4}m\pm R_c\cos\alpha\mp R_c\cos u)\sin\theta\boldsymbol{j}_t+(R_c\sin\alpha-R_c\sin u-R_g)\boldsymbol{k}_t\end{aligned}\tag{14}$$

The blank velocity at ***M*** comprises the rotation of the blank about its axis and the translational feed motion and is expressed as

$$\boldsymbol{n}_t \cdot \boldsymbol{v}_t = 0 \tag{15}$$

Therefore, the velocity of the cutter relative to the blank is

$$\phi = \boldsymbol{n}_t \cdot \boldsymbol{v}_g = \boldsymbol{e}_t \cdot \boldsymbol{v}_g = 0 \tag{16}$$

According to the axis directions shown in Figure 1, the relationship between the blank axis and the corresponding axis of St is

$$\boldsymbol{v}_g = w_g \boldsymbol{k}_g \times \boldsymbol{r}_g - w_g R_g \boldsymbol{i}_t = w_g (\boldsymbol{k}_g \times \boldsymbol{r}_g - R_g \boldsymbol{i}_t) \tag{17}$$

$$\begin{aligned}
&\boldsymbol{e}_t \cdot \boldsymbol{v}_g = (\cos u \cos\theta \boldsymbol{i}_t + \sin\theta \cos\theta \boldsymbol{j}_t \pm \sin u \boldsymbol{k}_t)\cdot \\
&\{w_g[(R_t \pm \frac{\pi}{4} m \pm R_c \cos\alpha \mp R_c \cos u)\cos\theta - R_g\psi - R_t]\boldsymbol{k}_t - \\
&w_g(R_c \sin\alpha - R_c \sin u - R_g)\boldsymbol{i}_t - w_g R_g \boldsymbol{i}_t\} \\
&= -w_g[R_c \cos\theta \sin(u-\alpha) + \sin u \cos\theta (R_t \pm \frac{\pi}{4} m) \mp \sin u (R_g\psi + R_t)]
\end{aligned} \tag{18}$$

Substitution of Equations (14)–(18) into the meshing condition in Equation (10) yields the meshing equation for the tooth surface generated by the convex or concave cutter:

$$R_c \cos\theta \sin(u-\alpha) + \sin u \cos\theta (R_t \pm \frac{\pi}{4} m) \mp \sin u (R_g\psi + R_t) = 0 \tag{19}$$

For a prescribed blank rotation angle φ, the common solution of the cutter swept-surface equation and the meshing equation defines the instantaneous cutter-workpiece contact line. As φ varies continuously, the instantaneous contact lines expressed in the moving blank coordinate system Sg envelope the theoretical tooth surface. The contact points must therefore be transformed from S_t to S_g. The homogeneous transformation matrix from St to the fixed workpiece coordinate system Sw is

$$M_{wt} = \begin{bmatrix} 1 & 0 & 0 & R_t \\ 0 & 0 & 1 & -R_g \\ 0 & -1 & 0 & 0 \\ 0 & 0 & 0 & 1 \end{bmatrix} \tag{20}$$

The homogeneous transformation matrix from S_w to the moving workpiece coordinate system S_g is

$$M_{gw} = \begin{bmatrix} \cos\psi & \sin\psi & 0 & R_g\psi\cos\psi \\ -\sin\psi & \cos\psi & 0 & -R_g\psi\sin\psi \\ 0 & 0 & 1 & 0 \\ 0 & 0 & 0 & 1 \end{bmatrix} \tag{21}$$

Accordingly, the cutter swept surface expressed in S_g is

$$\boldsymbol{r}_g^{(t)}(\varphi, \theta, u) = M_{gw} M_{wt} \boldsymbol{r}_t^{(t)} \tag{22}$$

Combining the convex and concave cutter swept-surface equations, the cutter-workpiece meshing equations, and the coordinate transformations gives the theoretical tooth surfaces of the driven and driving gears. Let r_{g2} and r_{g1} denote the position vectors of the driven- and driving-gear tooth surfaces, respectively. Then,

$$\begin{cases}
x_g = [(-R_t \mp \frac{\pi}{4} m \pm R_c \cos\alpha \mp R_c \cos u)\cos\theta + R_t + R_g\psi]\cos\psi - (R_c \sin\alpha - R_c \sin u + R_g)\sin\psi \\
y_g = [(-R_t \mp \frac{\pi}{4} m \pm R_c \cos\alpha \mp R_c \cos u)\cos\theta - R_t - R_g\psi]\sin\psi - (R_c \sin\alpha - R_c \sin u + R_g)\cos\psi \\
z_g = (-R_t \mp \frac{\pi}{4} m \pm R_c \cos\alpha \mp R_c \cos u)\sin\theta \\
R_c \cos\theta \sin(u-\alpha) + \sin u \cos\theta (R_t \pm \frac{\pi}{4} m) \mp \sin u (R_g\psi + R_t) = 0
\end{cases} \tag{23}$$

$$\begin{cases} x_g=[(-R_t\mp\dfrac{\pi}{4}m\mp R_c\cos\alpha\pm R_c\cos u)\cos\theta+R_t+R_g\psi]\cos\psi+(R_c\sin\alpha-R_c\sin u-R_g)\sin\psi \\ y_g=[(-R_t\mp\dfrac{\pi}{4}m\mp R_c\cos\alpha\pm R_c\cos u)\cos\theta-R_t-R_g\psi]\sin\psi+(R_c\sin\alpha-R_c\sin u-R_g)\cos\psi \\ z_g=(-R_t\mp\dfrac{\pi}{4}m\mp R_c\cos\alpha\pm R_c\cos u)\sin\theta \\ R_c\cos\theta\sin(u-\alpha)+\sin u\cos\theta(R_t\pm\dfrac{\pi}{4}m)\mp\sin u(R_g\psi+R_t)=0 \end{cases} \tag{24}$$

Equations (23) and (24) are parametric surface equations subject to the corresponding meshing constraints. The parameter u locates a contact point on a circular-arc cutting edge, φ describes the workpiece position during generation, and the cutter-head angle θ is determined from the meshing equation. Discrete points on the driving- and driven-gear tooth surfaces can thus be obtained by prescribing the parameter ranges and solving the corresponding meshing equations.

4. Effects of Geometric Parameters on Tooth-Surface Characteristics

4.1. Parameters and Evaluation Indices

Based on the tooth-surface model, a one-factor-at-a-time parametric analysis is performed to determine the effects of the number of teeth z, module m, pressure angle α, cutter profile arc radius R_c, root fillet coefficient r_{fc}, and rotary cutter-head radius R_t on the geometric characteristics of the C2CATT tooth surface. The middle-section tooth profile and tooth-trace geometric offset ΔX are selected as evaluation indices. The parameter ranges are listed in Table 1.

Table 1. Parameter Ranges of the C2CATT Gear.

Parameter	Range	Parameter	Range
Number of teeth	31–67	Cutter profile arc radius	300–600 mm
Module	2–5 mm	Root fillet coefficient	0.1–0.4
Pressure angle	18°–22°	Rotary cutter-head radius	150–450 mm

4.2. Effect of the Number of Teeth

Figure 3 shows the middle-section tooth profiles and tooth-trace geometric offsets obtained for different numbers of teeth while the other parameters are held at their reference values. As shown in Figure 3a, increasing the number of teeth from 31 to 67 changes the radial position and overall dimensions of the middle-section profile. After the profiles are aligned using the pitch-circle position as a common reference, their principal working portions nearly coincide. Thus, within the investigated range, the number of teeth has only a minor effect on the basic shape of the middle-section profile.

As shown in Figure 3b, the tooth-trace geometric-offset curves are symmetric about the mid-facewidth section. Their amplitudes are largest near the middle and gradually decrease toward both ends. The maximum offset amplitude decreases monotonically with increasing tooth number: ΔX is approximately 0.0275 mm at z = 31 and 0.0130 mm at z = 67, corresponding to a reduction of approximately 52.7%. The rate of decrease gradually diminishes as the number of teeth increases.

With the module, facewidth, and cutter-head radius fixed, increasing the tooth number enlarges the pitch radius of the blank and changes the relative curvature between the cutter swept surface and the blank. The spatial deflection over a fixed facewidth consequently decreases relative to the blank size, reducing the maximum tooth-trace offset amplitude. The number of teeth therefore primarily affects the spatial tooth-trace geometry and has a limited effect on the normalized middle-section tooth-profile shape.

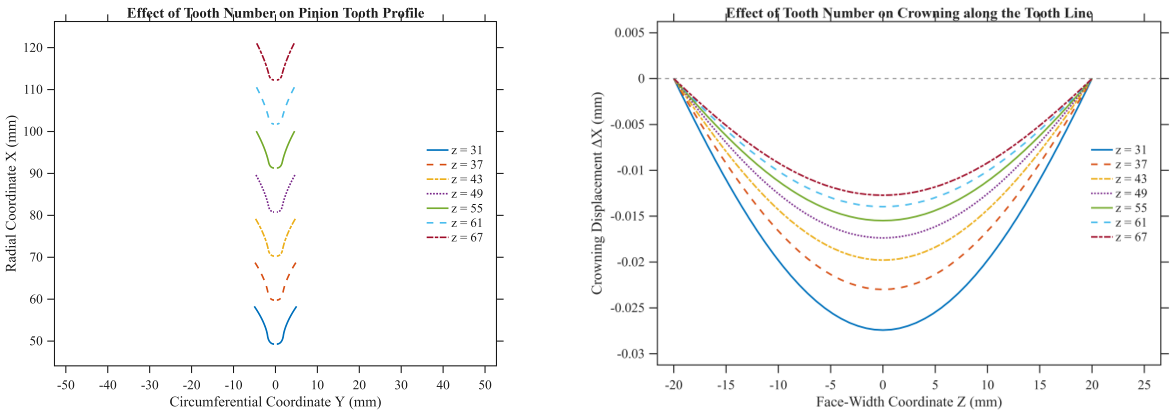

(a) Middle-section tooth profile **(b)** Tooth-trace geometric offset

Figure 3. Effect of the Number of Teeth on the Geometric Characteristics of the C2CATT Tooth Surface.

4.3. Effect of the Module

Figure 4 shows the middle-section tooth profiles and tooth-trace geometric offsets obtained for different modules while the other parameters are held at their reference values. As shown in Figure 4a, increasing the module from 2 to 5 mm increases the radial dimensions and tooth thickness, and shifts the overall profile radially outward. After alignment at the pitch-circle position, the profiles show similar trends over the principal working region, whereas the addendum and dedendum positions change more noticeably. Thus, within the investigated range, the module primarily controls tooth size and has a relatively small effect on the normalized shape of the working profile.

As shown in Figure 4b, the geometric-offset curves are symmetric about the mid-facewidth section, and their amplitudes gradually decrease from the middle toward both ends. The maximum amplitude increases with the module, from approximately 0.0150 mm at m = 2 mm to 0.0180 mm at m = 5 mm, corresponding to an increase of approximately 20.0%.

At a fixed number of teeth, increasing the module enlarges both the pitch radius and the characteristic tooth dimensions. Because the facewidth, cutter-head radius, and cutter profile arc radius remain fixed in this one-factor analysis, changing the module also changes the relative scale between the blank and cutter geometries. This modifies the spatial envelope relationship and increases the maximum tooth-trace offset amplitude. The module therefore determines the basic tooth dimensions and also affects the spatial tooth-trace geometry.

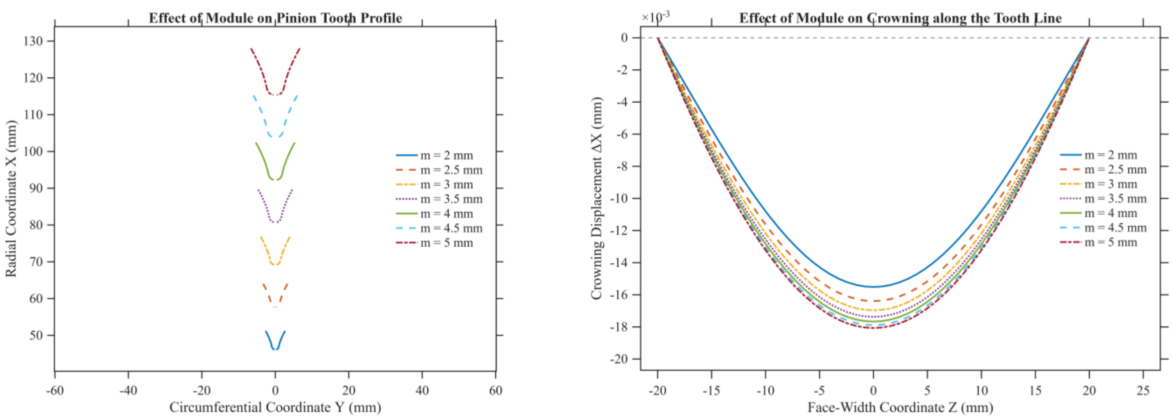

(a) Middle-section tooth profile **(b)** Tooth-trace geometric offset

Figure 4. Effect of the Module on the Geometric Characteristics of the C2CATT Tooth Surface.

4.4. Effect of the Pressure Angle

Figure 5 shows the middle-section tooth profiles and tooth-trace geometric offsets obtained for different pressure angles while the other parameters are held at their reference values. As shown in Figure 5a, the middle-section profile changes noticeably as the pressure angle increases from 18° to 22°. When the pitch-circle position is used as a common reference, the differences are relatively small near the pitch circle and increase toward the addendum and dedendum. A larger pressure angle increases the inclination of the working profile relative to the radial direction, decreases the tip thickness, and increases the tooth thickness near the root. The influence of the pressure angle is therefore nonuniform along the tooth height and is concentrated near the addendum and dedendum.

The pressure angle directly determines the basic orientation of the circular-arc cutting edge in the cutter axial section. A change in pressure angle alters the normal direction of the working edge and is transferred to the generated tooth surface through the cutter-workpiece envelope relationship, thereby changing the tip thickness, root thickness, and working-profile shape.

As shown in Figure 5b, the tooth-trace geometric-offset curves for different pressure angles are symmetric about the mid-facewidth section and follow similar trends. The pressure angle can therefore be used to adjust the sectional profile and the addendum and dedendum thicknesses, but it is not an effective primary parameter for controlling the tooth-trace offset. An excessively large pressure angle may produce an excessively thin or pointed tooth tip, whereas an excessively small pressure angle may reduce root thickness and increase the risk of undercutting or insufficient bending strength. Its value should therefore be selected by considering the minimum tip thickness, undercutting condition, and root bending strength.

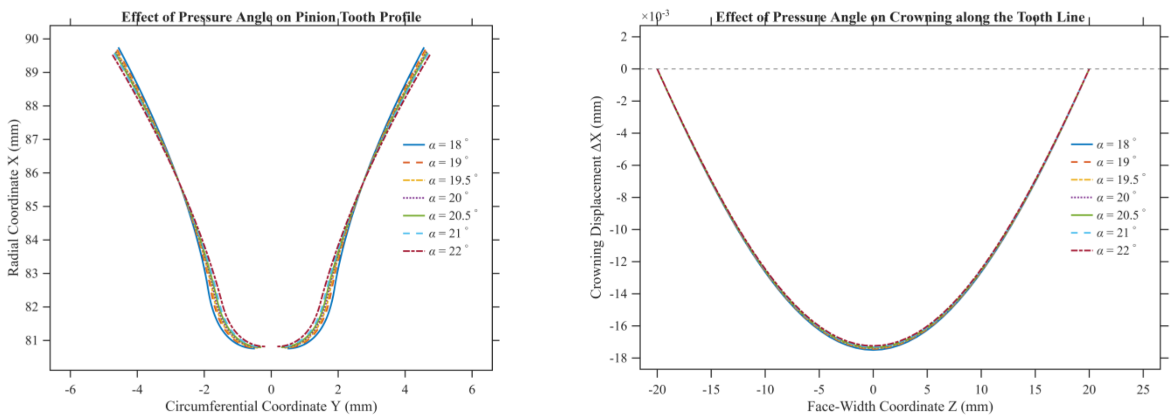

(a) Middle-section tooth profile **(b)** Tooth-trace geometric offset

Figure 5. Effect of the Pressure Angle on the Geometric Characteristics of the C2CATT Tooth Surface.

4.5. Effect of the Cutter Profile Arc Radius

Figure 6 shows the middle-section tooth profiles and tooth-trace geometric offsets obtained for different cutter profile arc radii while the other parameters are held at their reference values. As shown in Figure 6a, the principal portions of the profiles almost coincide when R_c varies from 300 to 600 mm, and the differences are concentrated near the addendum and dedendum. Increasing R_c reduces the curvature of the cutting-edge profile and, through the cutter-workpiece envelope relationship, changes the local curvature of the generated profile. Within the investigated range, R_c therefore mainly affects local profile geometry and has a relatively small effect on the overall position and principal shape of the profile.

As shown in Figure 6b, the tooth-trace geometric-offset curves obtained with different cutter profile arc radii are similar, and the maximum offset amplitude changes only slightly. This occurs because R_c mainly controls the cutting-edge curvature in the axial section, whereas the overall spatial geometry along the facewidth is governed primarily by the cutter-head radius, blank dimensions, and relative generating motion. Consequently, changing R_c does not markedly alter the overall distribution of tooth-trace geometric offset when the other parameters are fixed.

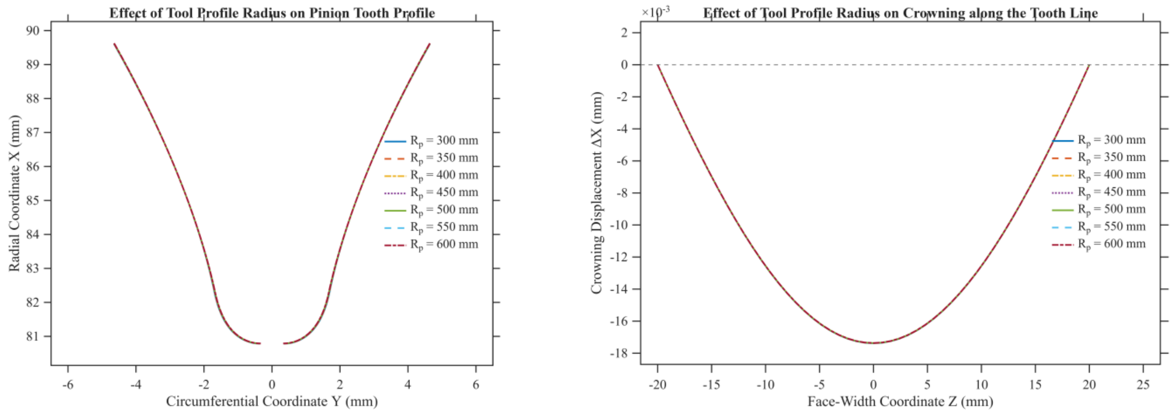

(a) Middle-section tooth profile **(b)** Tooth-trace geometric offset

Figure 6. Effect of the Cutter Profile Arc Radius on the Geometric Characteristics of the C2CATT Tooth Surface.

4.6. Effect of the Root Fillet Coefficient

Figure 7 shows the middle-section tooth profiles and tooth-trace geometric offsets obtained for different root fillet coefficients while the other parameters are held at their reference values. As shown in Figure 7a, when r_{fc} increases from 0.1 to 0.4, the profiles nearly coincide over the addendum and working-flank regions, whereas the differences are concentrated in the root transition. Increasing r_{fc} increases the root fillet radius and produces a smoother transition from the working flank to the root circle. Thus, the root fillet coefficient mainly controls the local root geometry and has little influence on the principal working portion of the middle-section profile.

As shown in Figure 7b, the tooth-trace geometric-offset curves for different root fillet coefficients nearly coincide, and the maximum offset amplitude remains essentially unchanged. The root fillet coefficient modifies only the cutter-tip fillet and the resulting root transition surface, without significantly changing the swept radius of the principal working edge or the overall cutter-workpiece kinematics. Therefore, within the investigated range, the root fillet coefficient has a limited effect on the overall tooth-trace geometry of the C2CATT tooth surface.

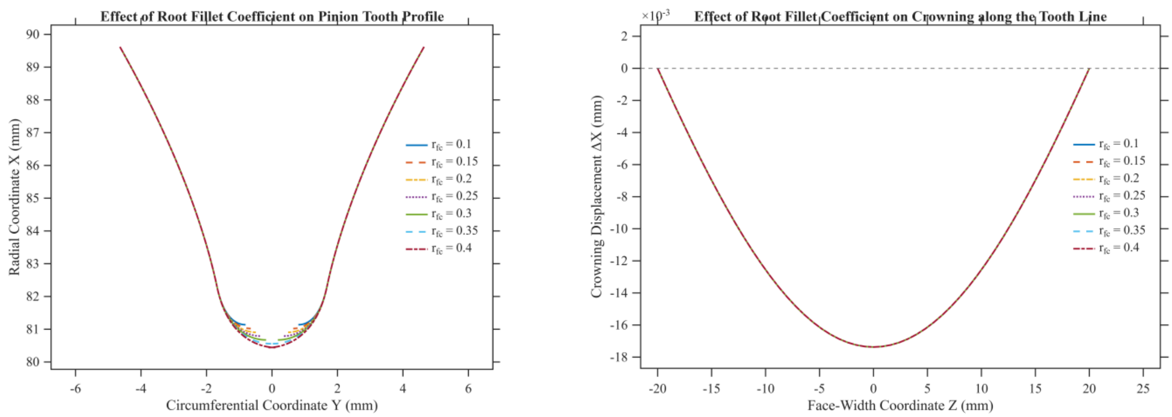

(a) Middle-section tooth profile **(b)** Tooth-trace geometric offset

Figure 7. Effect of the Root Fillet Coefficient on the Geometric Characteristics of the C2CATT Tooth Surface.

4.7. Effect of the Rotary Cutter-Head Radius

Figure 8 shows the middle-section tooth profiles and tooth-trace geometric offsets obtained for different rotary cutter-head radii while the other parameters are held at their reference values. As shown in Figure 8a, when R_t increases from 150 to 450 mm, the profiles nearly coincide over the addendum, working-flank, and root-transition regions. Thus, within the investigated range, the cutter-head radius has little influence on the middle-section tooth-profile shape.

As shown in Figure 8b, the tooth-trace geometric-offset curves remain symmetric about the mid-facewidth section, but their amplitudes differ markedly. The maximum offset amplitude decreases continuously with increasing R_t, indicating that the cutter-head radius is a principal parameter controlling the spatial tooth-trace geometry. A smaller cutter-head radius produces a more highly curved cutting-edge trajectory and larger positional differences among sections across the facewidth. As R_t increases, the trajectory becomes flatter and the geometric offset between the middle and both ends decreases.

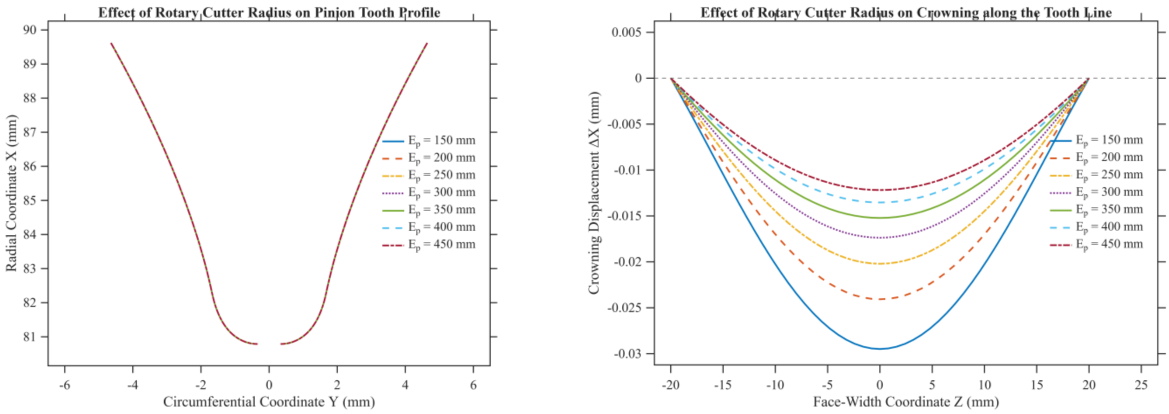

(a) Middle-section tooth profile **(b)** Tooth-trace geometric offset

Figure 8. Effect of the Rotary Cutter-Head Radius on the Geometric Characteristics of the C2CATT Tooth Surface.

The rotary cutter-head radius can therefore be used to adjust tooth-trace curvature and spatial offset. A smaller radius produces a more pronounced spatial curvature, whereas a larger radius produces a flatter tooth trace. However, selection of Rt is also constrained by machine-tool dimensions, cutter installation space, and available travel, and should balance the target tooth-trace geometry against manufacturing-equipment constraints.

4.8. Overall Comparison

To compare the effects of the investigated parameters on the spatial tooth-trace geometry, Figure 9 presents the variation in the maximum tooth-trace geometric-offset amplitude ΔX for each parameter.

As shown in Figure 9a, ΔX decreases monotonically with the number of teeth. Increasing the tooth number from 31 to 67 reduces ΔX from approximately 0.0275 to 0.0130 mm, a decrease of approximately 52.7%, and the rate of decrease gradually diminishes. As shown in Figure 9b, increasing the module from 2 to 5 mm increases ΔX from approximately 0.0150 to 0.0180 mm, corresponding to an increase of approximately 20.0%.

Figure 9c,d show that, within the investigated ranges, variations in the pressure angle and cutter profile arc radius cause only small changes in ΔX. The pressure angle mainly affects the addendum, dedendum, and working profile of the middle section, whereas the cutter profile arc radius primarily controls local profile curvature. Neither parameter is a primary control variable for the overall tooth-trace offset. Figure 9e shows that ΔX remains almost unchanged with the root fillet coefficient, confirming that this parameter mainly affects the local root transition.

As shown in Figure 9f, the cutter-head radius has a pronounced effect on ΔX. Increasing Rt from 150 to 450 mm continuously reduces ΔX because the cutter-head radius directly controls the curvature of the cutting-edge trajectory. A larger radius produces a flatter trajectory over the facewidth and therefore reduces the positional difference between the middle and both ends.

Within the investigated parameter ranges, the number of teeth and cutter-head radius produce the most pronounced variations in the maximum tooth-trace offset amplitude, followed by the module; the effects of the pressure angle, cutter profile arc radius, and root fillet coefficient on this particular index are relatively weak. Nevertheless, the parameters affect different aspects of the tooth-surface geometry: the tooth number and cutter-head radius mainly control the spatial tooth-trace geometry; the module affects both tooth size and tooth-trace offset; the pressure angle controls the middle-section profile and tooth-thickness distribution; the cutter profile arc radius affects local profile curvature; and the root fillet coefficient controls the root transition. Parameter importance should therefore be assessed against the target geometric characteristic rather than solely from ΔX.

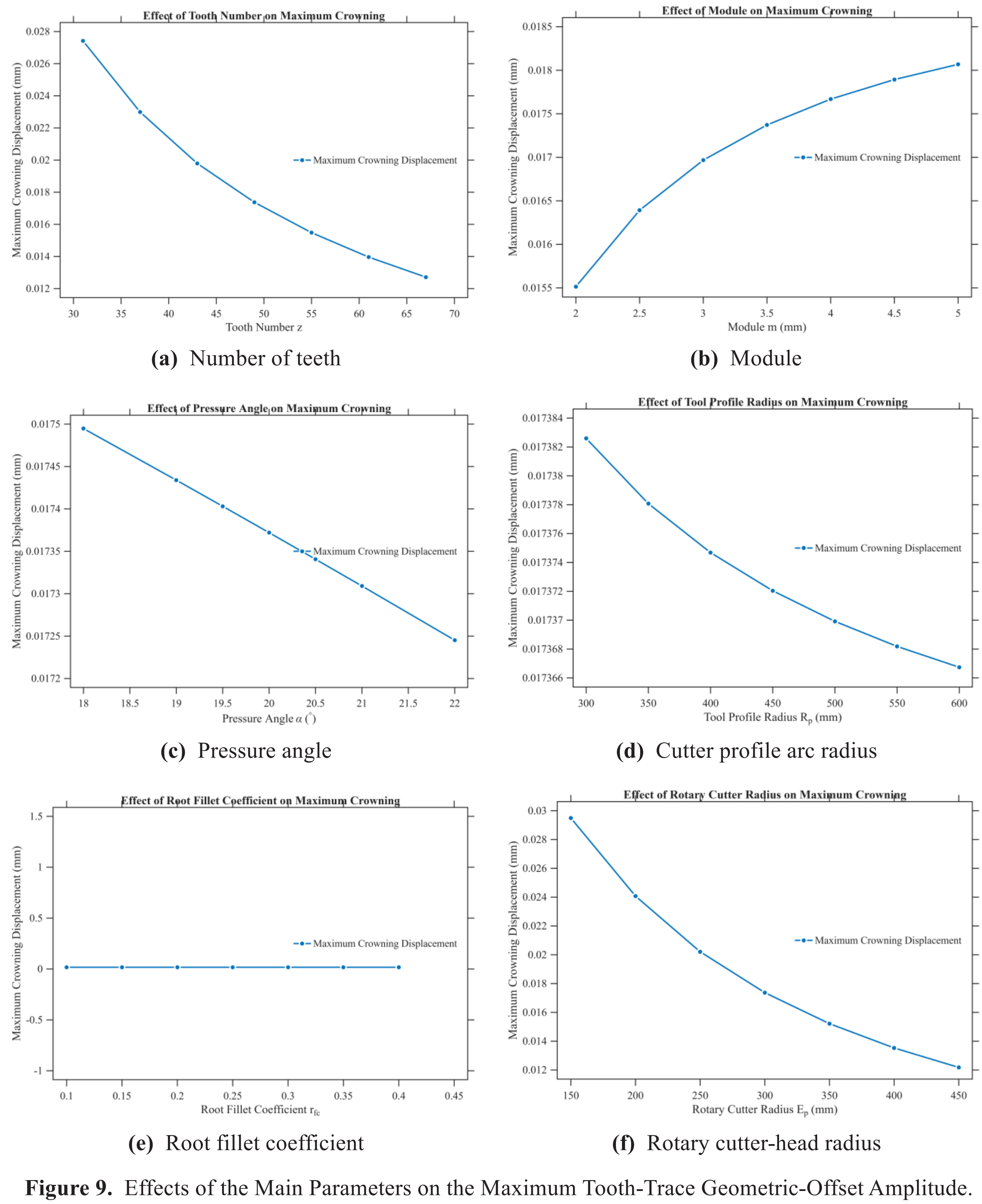

(a) Number of teeth

(b) Module

(c) Pressure angle

(d) Cutter profile arc radius

(e) Root fillet coefficient

(f) Rotary cutter-head radius

Figure 9. Effects of the Main Parameters on the Maximum Tooth-Trace Geometric-Offset Amplitude.

5. Conclusions

A circular-arc-profile and circular-arc-tooth-trace cylindrical gear is proposed, and its machining principle and tooth-surface mathematical model are established. The effects of the principal parameters on its geometric characteristics are analyzed. The main conclusions are as follows.

(1) A complementary pair of locally conjugate convex and concave circular-arc cutters is designed to generate the driving- and driven-gear tooth surfaces, respectively. By matching the local geometry of the mating tooth surfaces at the design position, the cutter configuration provides a geometric basis for a controllable localized-contact gear pair.

(2) Based on the dual-edge rotary cutter-head machining principle and spatial envelope theory, the swept-surface equations of the convex and concave cutters, the cutter-workpiece meshing equations, and the coordinate transformations are established. Parametric equations for the driving- and driven-gear tooth surfaces are obtained, establishing a mathematical relationship between cutter parameters and the generated surfaces.

(3) The geometric offset of the C2CATT tooth surface is symmetric about the mid-facewidth section, and its

amplitude decreases from the middle toward both ends. Within the investigated ranges, the number of teeth and cutter-head radius have pronounced effects on the maximum offset amplitude, followed by the module. Increasing the tooth number from 31 to 67 reduces the maximum amplitude from approximately 0.0275 to 0.0130 mm, a decrease of 52.7%; increasing the module from 2 to 5 mm increases it from approximately 0.0150 to 0.0180 mm, an increase of 20.0%. Increasing the cutter-head radius reduces the tooth-trace geometric-offset amplitude.

(4) The parameters affect different geometric characteristics. The pressure angle primarily affects the middle-section profile and the addendum and dedendum thicknesses; the cutter profile arc radius mainly affects local profile curvature; and the root fillet coefficient controls the root transition. The latter two parameters have relatively small effects on the overall tooth-trace offset. These relationships provide guidance for tooth-surface design and cutter parameter selection for C2CATT gears.

Funding

This work was supported by the Sichuan Science and Technology Program (Project No. 2023ZYD0139), the Natural Science Foundation of Sichuan Province (Project No. 2022NSFSC0454, 2022NSFSC1975).

Author Contributions

Conceptualization, L.H.; methodology, Q.Z.; software, Q.Z.; formal analysis, Q.Z.; investigation, Q.Z.; resources, Q.Z.; writing—original draft preparation, Q.Z.; writing—review and editing, L.H.; visualization, Q.Z.; supervision, L.H.; Funding acquisition, Q.Z. All authors have read and agreed to the published version of the manuscript.

Institutional Review Board Statement

Not applicable.

Informed Consent Statement

Not applicable.

Data Availability Statement

No supplementary or additional data were generated in this study.

Conflicts of Interest

The authors declare no conflicts of interest.

References

1 Wu Y-C, Chen KY, Tsay C-B, *et al.* Contact Characteristics of Circular-Arc Curvilinear Tooth Gear Drives. *Journal of Mechanical Design* 2009; **131**: 081003. https://doi.org/10.1115/1.3151805.

2 Peng Y, Song A, Shen Y, *et al.* A Novel Arc-Tooth-Trace Cycloid Cylindrical Gear. *Mechanism and Machine Theory* 2017; **118**: 180–193. https://doi.org/10.1016/j.mechmachtheory.2017.08.009.

3 Zhang Q, Hou L, Tang R, *et al.* Method of Processing and an Analysis of Meshing and Contact of Circular Arc Tooth Trace Cylindrical Gears. *Transactions of FAMENA* 2016; **40**: 11–24. https://doi.org/10.21278/TOF.40402.

4 Liang S, Luo P, Hou L, *et al.* Research on Processing Error of Special Machine Tool for VH-CATT Cylindrical Gear. *Machines* 2022; **10**: 679. https://doi.org/10.3390/machines10080679.

5 Liang S, Hou L, Zhang H, *et al.* Bifurcation and Chaos Analysis of Cutter Head-Spindle System of VH-CATT Gear Machine Tool Considering Time-Varying Stiffness. *The International Journal of Advanced Manufacturing Technology* 2023; **124**: 3995–4008. https://doi.org/10.1007/s00170-021-08360-0.

6 Liang S, Wu Y, Hou L, *et al.* Research on Influence Mechanism of Geometric Error Sources on Tooth Surface Error of VH-CATT Gear Special Machine Tool. *The International Journal of Advanced Manufacturing Technology* 2023; **128**: 5529–5546. https://doi.org/10.1007/s00170-023-12001-z.

7 Wang S, Hou L, Dong L, *et al.* Manufacturing-Oriented Modeling and Strength Analysis of an Arc-Tooth Cylindrical Gear. *Journal of Sichuan University (Engineering Science Edition)* 2012; **44**: 210–215. https://doi.org/10.15961/j.jsuese.2012.02.029. (in Chinese)

8 Zhao F, Hou L, Duan Y, *et al.* Forming Theory and Digital Modeling of a Circular-Arc Gear Generated by a Rotary Cutter. *Journal of Sichuan University (Engineering Science Edition)* 2016; **48**: 119–125. https://doi.org/10.15961/j.jsuese.2016.06.017. (in Chinese)

9 Zhao F, Hou L, Chen Y, *et al.* Complete Tooth-Surface Mathematical Model and Analysis of Cutting Conditions for Circular-Arc-Tooth-Trace Cylindrical Gears. *Journal of Jilin University (Engineering and Technology Edition)* 2020; **50**: 875–885. https://doi.org/10.13229/j.cnki.jdxbgxb20190058. (in Chinese)

10 Chen B, Gao Y, Liang D. Construction of Tooth Surfaces for Conjugate-Curve Gears. *Journal of Mechanical Engineering* 2014; **50**: 18–24. https://doi.org/10.3901/JME.2014.03.018. (in Chinese)

11 Luo L, Hou L, Zhao F, *et al.* Geometric Characteristics of Variable-Hyperbolic Circular-Arc-Tooth-Trace Cylindrical Gear Transmission. *Advanced Engineering Sciences* 2018; **50**: 171 – 179. https://doi. org/10. 15961/j.jsuese.201700511. (in Chinese)

12 Ma D, Ye Z, Yang H. Tooth Surface Reconstruction and Tooth Profile Geometric Analysis of Circular Arc Tooth Trace Cylindrical Gears. *Transactions of FAMENA* 2019; **43**: 29–44. https://doi.org/10.21278/TOF.43103.

13 Jiang B, Ren Z, Duan J, *et al.* Modeling and Load-Carrying Capacity Analysis of a Circular-Arc-Profile and Circular-Arc-Tooth-Trace Cylindrical Gear. *Journal of Mechanical Strength* 2022; **44**: 742–746. https://doi.org/10.16579/j.issn.1001.9669.2022.03.033. (in Chinese)

14 Wu Y, Hou L, Luo L, *et al.* Research on the Effect Law of Machine Tool Errors on Tooth Surface Errors of Curvilinear Gear. *Journal of Mechanical Engineering* 2020; **56**: 100–109. https://doi.org/10.3901/JME.2020.21.100. (in Chinese)

15 Wei Y, Li Z, Liu Y, *et al.* Geometric Contact Characteristics and Sensitivity Analysis of a Variable-Hyperbolic circular-Arc-Tooth-Trace Cylindrical Gear Considering Errors. *Journal of Northwestern Polytechnical University* 2022; **40**: 679–689. https://doi.org/10.1051/jnwpu/20224030679. (in Chinese)

16 Wei Y, Wang Y, Li Z, *et al.* Geometric Contact Characteristics of Variable Hyperbolic Circular-Arc-Tooth-Trace Cylindrical Gear under Different Machine Tool Errors and Sensitivity Analysis for Impact Factors. *The Journal of Strain Analysis for Engineering Design* 2024; **59**: 269 – 280. https://doi. org/10.1177/03093247241232865.

17 Ma D, Jiang B, Bao L, *et al.* Study on the Contact Performance of the Variable Hyperbolic Circular Arc Tooth Trace Cylindrical Gear with Installation Errors. *Mechanical Sciences* 2024; **15**: 353–366. https://doi.org/10.5194/ms-15-353-2024.

18 Guo R, Wei Y, Liu Y, *et al.* Analytical Solution to Contact Characteristics for a Variable Hyperbolic Circular-Arc-Tooth-Trace Cylindrical Gear. *Mechanical Sciences* 2021; **12**: 923–932. https://doi.org/10.5194/ms-12-923-2021.

19 Ma D, Liu Y, Ye Z, *et al.* Analysis of the Tooth Surface Contact Area of a Circular-Arc-Tooth-Trace Cylindrical Gear Under Load. *Transactions of FAMENA* 2021; **45**: 79–94. https://doi.org/10.21278/TOF.451018220.

20 Ma D, Liu Y, Ye Z, *et al.* Modification Design and Loaded Tooth Contact Analysis of Variable-Hyperbolic Circular-Arc-Tooth-Trace Cylindrical Gears. *Journal of Vibration and Shock* 2023; **42**: 170–179. (in Chinese).

21 Zhang Q, Chen Z, Wu Y, *et al.* Contact Stress Reliability Analysis Model for Cylindrical Gear with Circular Arc Tooth Trace Based on an Improved Metamodel. *Computer Modeling in Engineering & Sciences* 2024; **140**: 593–619. https://doi.org/10.32604/cmes.2023.046319.

22 Ma D, Ye Z. Nonlinear Dynamic Characteristics of Modified Variable Hyperbolic Circular Arc Tooth Trace Cylindrical Gears. *Scientific Reports* 2025; **15**: 15108. https://doi.org/10.1038/s41598-025-97254-2.

23 Ma D, Long J, Zhu Z. Meshing Characteristics of Variable Hyperbolic Circular-Arc Tooth Trace Cylindrical Gears with Cutter Errors. *Mechanical Sciences* 2025; **16**: 475–491. https://doi.org/10.5194/ms-16-475-2025.

© The Author(s) 2026. Published by Global Science Publishing (GSP).

This is an Open Access article distributed under the terms of the Creative Commons Attribution License (https://creativecommons.org/licenses/by/4.0), which permits unrestricted use, distribution, and reproduction in any medium, provided the original work is properly cited.